



New chiral discotics with helical organization of the mesophase—liquid crystalline derivatives of dibenzotetraaza[14]annulene

Jarosław Grolik^a, Łukasz Dudek^a, Julita Eilmes^{a,*}, Andrzej Eilmes^a, Marcin Górecki^b, Jadwiga Frelek^b, Benoît Heinrich^c, Bertrand Donnio^c

^a Department of Chemistry, Jagiellonian University, Ingardena 3, 30-060 Kraków, Poland

^b Institute of Organic Chemistry of the Polish Academy of Sciences, Kasprzaka 44, 01-224 Warszawa, Poland

^c Institut de Physique et Chimie des Matériaux de Strasbourg, CNRS-Université de Strasbourg (UMR7504), BP 43, F-67034 Strasbourg Cedex 2, France

ARTICLE INFO

Article history:

Received 23 November 2011

Received in revised form 26 February 2012

Accepted 12 March 2012

Available online 20 March 2012

Keywords:

Dibenzotetraaza[14]annulene

Liquid crystals

SA-XRD

Supramolecular chirality

ECD spectroscopy

Molecular Dynamics

ABSTRACT

Two optically pure derivatives of dibenzotetraaza[14]annulene, bearing four (*S*)- or (*R*)- 3,7-dimethyloctoxy peripheral chiral tails, respectively, and two hydroxybenzoyl *meso* substituents were synthesized using a convergent multi-step route. The structure of the products was determined by ¹H and ¹³C NMR spectroscopy, ESI-MS, and elemental analysis. The mesomorphic behavior of the two chiral compounds, deciphered by differential scanning calorimetry (DSC), small-angle X-ray diffractometry (SA-XRD), and polarizing optical microscopy (POM) investigations, revealed the induction of two lamello-columnar phases, i.e., columnar stacks confined in smectic layers, whose columns may be arranged either according to the *pg* rectangular planar symmetry (for the low-temperature phase) or without registry between vicinal layers (for the high-temperature mesophase). Evidence of a helical organization of the molecules in the mesophases was obtained using a combination of electronic circular dichroism (ECD) and SA-XRD results, Molecular Dynamics simulations and quantum-chemical calculations.

© 2012 Elsevier Ltd. All rights reserved.

1. Introduction

Much interest in liquid crystalline materials arises from their potential application as active components in organic electronics.¹ In particular, mesogens based on chiral disc-like molecules have recently attracted considerable attention as systems exhibiting a helical supramolecular organization of the mesophase and therefore responsible for a number of interesting properties.² Thus, ferroelectric switching,³ high charge-carrier mobility,⁴ and exceptional second order nonlinear optical susceptibilities⁵ were found to be associated in columnar discotic mesophases with a helical architecture.

A number of known discotic liquid crystals are based on macrocyclic compounds containing extended aromatic cores and large polyaromatic hydrocarbons (PAH), and show an intrinsically high tendency to aggregate into infinite one-dimensional columnar stacks.¹ Typically, porphyrins,⁶ phthalocyanines,⁷ hexabenzocoronenes,⁸ and triphenylenes,⁹ equipped with flexible peripheral paraffinic tails, represent this type of discotic mesogen. Among these systems, those containing stereogenic centers in the

peripheral chains are likely to exhibit a helical superstructure of the columnar mesophases.^{2,10} It should be noted, however, that helical self-assembly in the liquid crystalline columnar phases may also originate from other molecular characteristics, such as shape and topology.^{2,11}

We have recently shown that the dibenzotetraaza[14]annulene (DBTAA) ligand **1** (Fig. 1), substituted at the periphery by pro-

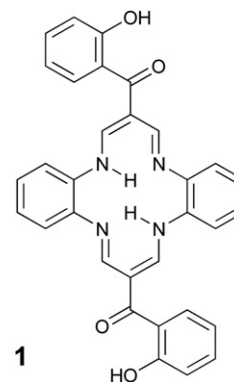


Fig. 1. Dibenzotetraaza[14]annulene (DBTAA) **1**.¹⁷

* Corresponding author. Tel.: +48 12 6632294; fax: +48 12 6340515; e-mail address: jeilmes@chemia.uj.edu.pl (J. Eilmes).

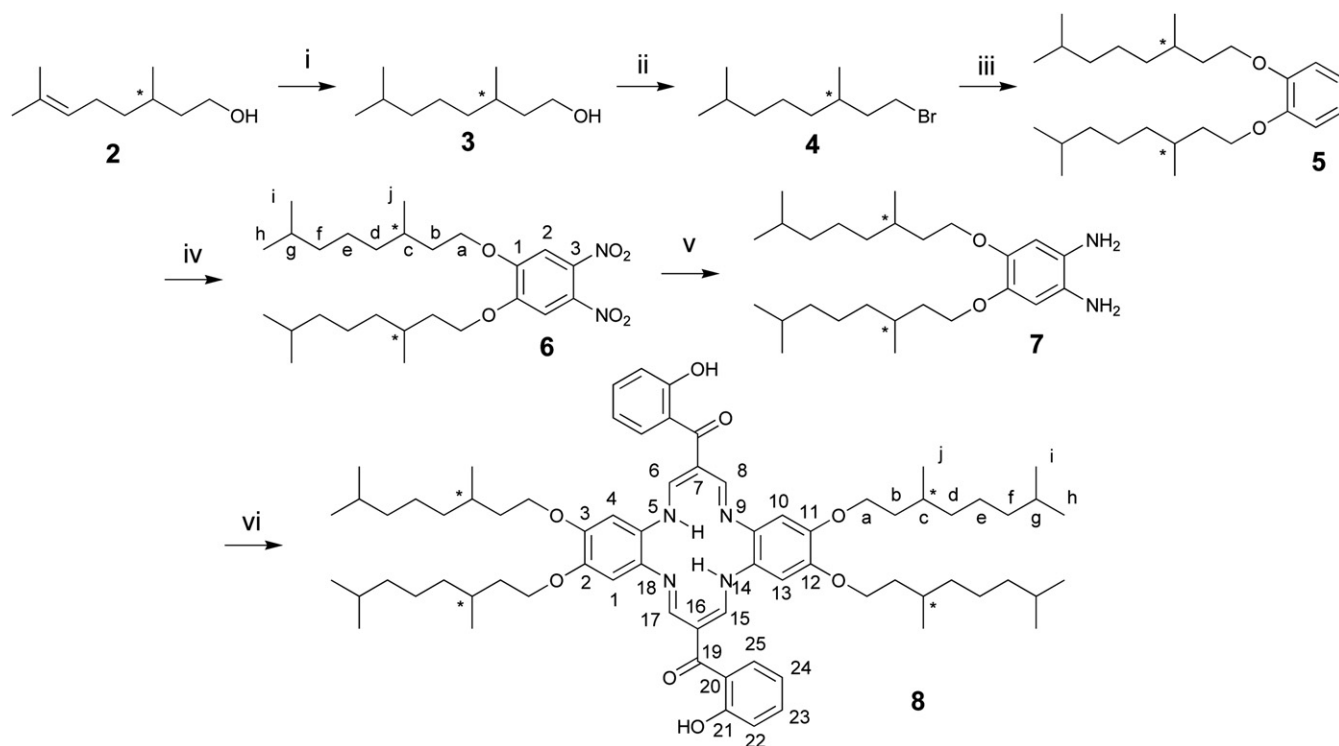
mesogenic paraffinic tails, gives rise to materials exhibiting columnar mesomorphism driven by π – π interactions.¹² The DBTAA core in **1** is nearly flat, and rich in π delocalized areas; therefore it seems to be well suited to play the role of a disc-shaped tecton. In addition, peripheral reactivity and the capability of accommodating various substituents on the phenylene rings and imine carbons make this system very attractive for the design and synthesis of materials-directed building blocks.

Here, we report our results in preparing DBTAA-based discotic liquid crystals with a helical architecture of the mesophase. In order to promote helical self-assembly of the molecules in columnar phases, we have designed and synthesized new optically pure, chiral derivatives **8** of DBTAA (Scheme 1).

2. Results and discussion

2.1. Synthesis

The synthetic pathway to chiral derivatives of DBTAA, (all-*S*)-**8** and (all-*R*)-**8**, is summarized in Scheme 1. The method involves the initial preparation of optically pure (*R,R*)- and (*S,S*)-4,5-bis(3,7-dimethyloctoxy)-*o*-phenylenediamine **7** using a multi-step route involving the alkylation of catechol with the appropriate chiral alkyl bromide **4**, followed by nitration of the products.^{15,16} The (*S,S*)- and (*R,R*)-1,2-dinitro-4,5-bis(3,7-dimethyloctoxy)benzenes **6** were reduced by means of NaBH₄/methanol in the presence of 10% Pd/C and the corresponding diamines **7** were then condensed with 3-



Scheme 1. Reagents and conditions: (i) H₂, 10% Pd/C, methanol, rt, 24 h, (41–53%); (ii) NBS, Ph₃P, CH₂Cl₂, rt, 16 h, (68–74%); (iii) catechol, K₂CO₃, DMF, 80 °C, 5 h, (56–61%); (iv) (1) CH₂Cl₂, HNO₃, rt, 30 min, (2) H₂SO₄, rt, 1.5 h, (65–76%); (v) 10% Pd/C, NaBH₄, methanol, 65 °C; (vi) 3-formylchromone, methanol, 65 °C, 1 h, (36–41%).

The designed molecule **8** contains four peripheral (*R*)- or (*S*)-3,7-dimethyloctoxy substituents attached to the phenylene fragments, and two 2-hydroxybenzoyl groups located at the *meso* positions of the macrocyclic ring. In our strategy, we took into account crystallographic results, showing that 2-hydroxybenzoyl *meso* substituents in **1** and in other derivatives of **1** were non-coplanar arranged with respect to the main plane of the macrocycle, and that phenolic OH groups in these moieties were engaged in effective H-bonding interactions.^{12,13} Therefore, in view of the structural data of known helically organized mesogens,¹⁴ we expected that both the steric requirements and chirality associated with the substituents in **8** may force the molecules to self-assemble in a helical fashion. Stabilization of the resulting helicoidal arrangement of the mesogens within the supramolecular structures through H-bonding interactions seemed also probable.

The new material was fully characterized by means of ¹H and ¹³C NMR spectroscopy, ESI-MS, and elemental analysis and their thermal behavior and mesophase structures were analyzed by means of differential scanning calorimetry (DSC), thermogravimetry (TGA), X-ray diffractometry (XRD), polarizing optical microscopy (POM), and circular dichroism (CD).

formylchromone to give optically pure (all-*S*)-**8** and (all-*R*)-**8**, following a general procedure reported earlier.¹⁷

(*S*)-3,7-Dimethyl-1-octanol **3** was prepared by hydrogenation of commercially available (*S*)-(-)-β-Citronellol, and next transformed to the bromide (*S*)-**4**.^{18,19} In order to prepare the corresponding (*R*)-3,7-dimethyl-1-octanol **3**, (*R*)-(+)-β-Citronellol was first synthesized starting from (*R*)-(+)-Pulegone according to the procedure described in the literature.¹⁸

2.2. Thermal behavior (POM, TGA, DSC)

The thermal behavior of (all-*S*) and (all-*R*)-**8**, as well as of the racemic (*rac*)-**8** prepared previously,¹² was first investigated by the use of POM, TGA, and DSC.

On heating, several phase transitions were detected before clearing in the isotropic liquid at 192 °C. Characteristic optical textures of discotic columnar phases (e.g., large growing cylindrical monodomains, broken fan texture, dendrites) were observed under polarized light microscopy for all studied compounds ((*rac*)-**8**,¹² (all-*S*)-**8**, and (all-*R*)-**8**). The photographs were taken during heating, and on slow cooling to lower temperatures after annealing the

sample for a few minutes at high temperature, in the isotropic liquid near the decomposition temperature. Examples of typical textures obtained under these conditions are shown in Fig. 2.

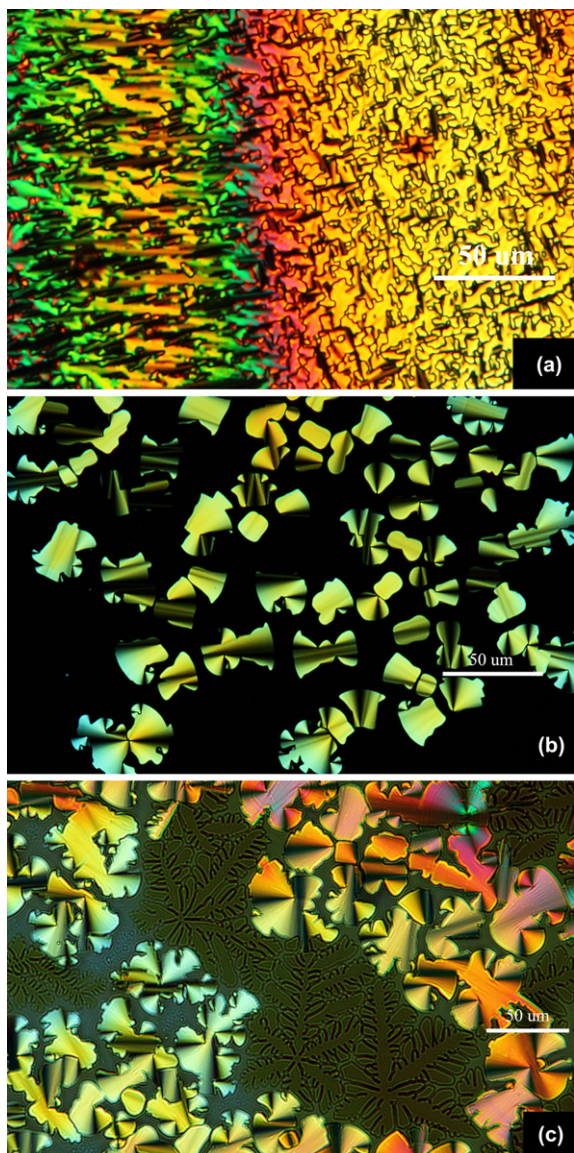


Fig. 2. Optical textures of compound (all-S)-8 observed using polarized light microscopy: (a) at 112.0 °C (heating 0.1 °C/min, 10 \times , crossed polarizers); (b) at 162.0 °C (cooling 5 °C/min, 10 \times , crossed polarizers); (c) at -4.5 °C (cooling 5 °C/min, 10 \times , crossed polarizers).

Textures of both mesophases on cooling exhibit defects consistent with columnar organizations. Homeotropic domains in the high-temperature phase, indicative of uniaxiality, are replaced by weakly birefringent areas in the phase below, which is either uniaxial or weakly biaxial (Fig. 2).

The thermal stability of the samples was checked using TGA. As shown in Fig. S1 (Supplementary data), both the racemic mixture, (*rac*)-8, and the stereoisomer (all-S)-8 are thermally stable up to 200 °C, at which a small weight-loss is detected (~ 0.5 wt%). Then above this temperature, ca. 210–220 °C, the samples begin to lose weight continuously, and at temperatures higher than 250 °C, the compounds are fully degraded.

The DSC data (Fig. S2, Supplementary data) show that (*rac*)-8 only exhibits one measurable, quite broad, transition, at ca. 80 °C, corresponding to a transition between two mesophases, as shown by the small temperature shift ($\Delta T \approx 4$ °C) and the small enthalpy change ($\Delta H \sim 2$ J g $^{-1}$). The clearing transition is not detected by DSC (the onset of the clearing being determined by POM only at 192 °C) and is consistent with the slow and progressive transition resulting in a broadened signal spread over several degrees, with non-resolvable enthalpy. This thermal behavior is fully reproducible on subsequent heat-cool cycles, providing that the decomposition temperature is not reached.

The pure enantiomers exhibit indistinguishable thermal behaviors from one another, but markedly different to that of the racemic material (*rac*)-8. During the first heating, DSC traces of both (all-S)-8 and (all-R)-8 exhibit two sharp endothermic peaks, a very intense one at ca. 79–80 °C, attributed to the melting transition into a mesophase (ΔH of the order of 20 J g $^{-1}$) and another one at ca. 114–115 °C with a much smaller enthalpy change ($\Delta H \sim 6$ –7 J g $^{-1}$), likely accounting for a mesophase-to-mesophase transformation; as above, due to a slow and progressive isotropization, the transition corresponding to the clearing event has not been detected (Fig. 3). On cooling, the transition temperature between the two mesophases is slightly shifted, by ca. 5–6 °C (Fig. 4). No other thermal event was detected below 0 °C but on subsequent heating (second and third), a small transition (7–8 °C), which is attributed to the melting of partially crystalline solid into the mesophase (Fig. 4) is observed; this behavior is fully reversible.

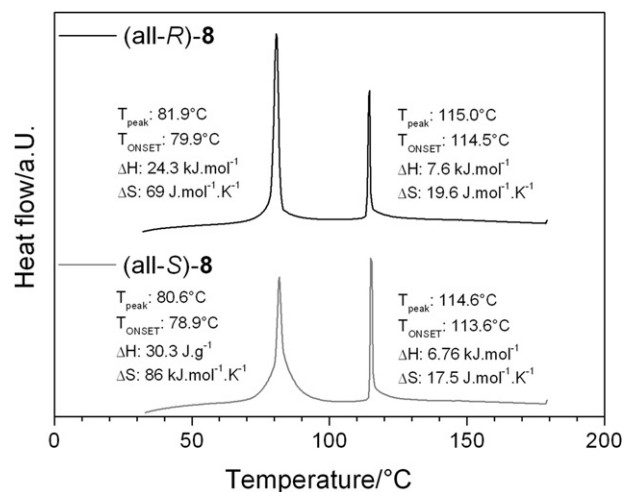


Fig. 3. DSC traces of the first heating of (all-R)-8 and (all-S)-8.

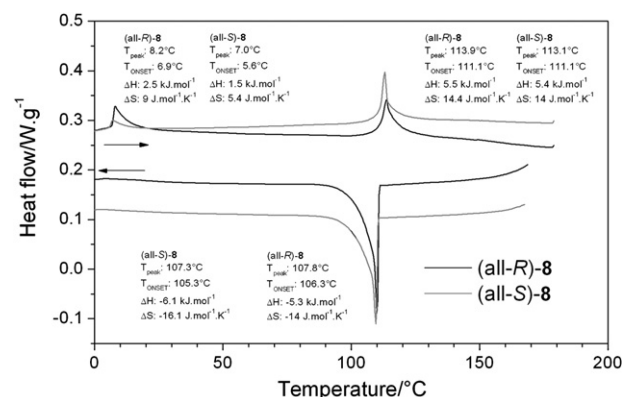


Fig. 4. DSC traces of (all-R)-8 and (all-S)-8 (first cool and second heat).

2.3. X-ray diffraction

The thermal behaviors recorded by DSC fully match the small-angle diffraction experiments performed at variable temperatures. XRD results confirm that the various transition temperatures detected by DSC correspond effectively to phase changes (with the formation of two lamello-columnar mesophases), and that the three compounds decompose above 200 °C. At room temperature, the two isomers are crystalline. In contrast, the racemic mixture (*rac*)-**8** is not as prone to crystallization, probably owing to the fact that the stereoisomers cannot pack together in the same crystal lattice and the coexistence of several crystalline phases in the solidified mixtures implies a crystallization onset temperature considerably lowered with respect to that of the pure isolated isomers. As shown by SA-XRD, the same low-temperature mesophase, with almost similar lattice parameters, is present for the three compounds (Table 1, Fig. 5). In the wide angle region, the intense and unusually slightly broadened reflection at 3.35 Å (h_0) evidences the

Table 1
XRD data for (*rac*)-**8**, (*all-S*)-**8**, and (*all-R*)-**8**

Compounds	$d_{\text{exp}}/\text{Å}^a$	$[hkl]^b$	I^c	$d_{\text{theo}}/\text{Å}^{a,d}$	Parameters ^{d,e}
<i>(rac)</i> - 8	21.86	11	vs (sh)	21.9	$T=60\text{ °C}$
	18.0	20	m (sh)	18.0	LamCol _r -pg
	12.7	12	w (sh)	12.85	$a=36.0\text{ Å}, b=27.5\text{ Å}$
	4.8	h_{h1}	vs (br)	Alkyl chains	$S=990\text{ Å}^2$
	4.1	h_{h2}	vs (br)	Alkyl chains	$h=3.83\text{ Å}$
	3.35	h_0	vs (sh)	π -Stacking	$Z=2, N=1$
	21.76	001	vs (sh)	21.76	$T=140\text{ °C}$
	4.5	h_h	s (br)	Alkyl chains	LamCol
	3.5	h_0	s (sh)	π -Stacking	$d=21.76\text{ Å}$
					$A=87.3\text{ Å}^2$
<i>(all-S)</i> - 8	22.12	11	vs (sh)	22.12	$T=80\text{ °C}$
	18.06	20	s (sh)	18.06	LamCol _r -pg
	12.75	12	w (sh)	13.05	$a=36.1\text{ Å}, b=27.95\text{ Å}$
	4.8	h_{h1}	vs (br)	Alkyl chains	$S=1009\text{ Å}^2$
	4.2	h_{h2}	s (sh)	Alkyl chains	$h=3.75\text{ Å}$
	3.35	h_0	s (sh)	π -Stacking	$Z=2, N=1$
	21.8	001	vs (sh)	21.75	$T=140\text{ °C}$
	10.85	002	w (sh)	10.9	LamCol
	4.5	h_h	vs (br)	Alkyl chains	$d=21.75\text{ Å}$
	3.5	h_0	vs (sh)	π -Stacking	$A=87.35\text{ Å}^2$
<i>(all-R)</i> - 8	22.1	11	vs (sh)	22.1	$T=80\text{ °C}$
	18.05	20	s (sh)	18.05	LamCol _r -pg
	12.86	12	w (sh)	13.03	$a=36.12\text{ Å}, b=28.0\text{ Å}$
	4.8	h_{h1}	vs (br)	Alkyl chains	$S=1011\text{ Å}^2$
	4.2	h_{h2}	s (sh)	Alkyl chains	$h=3.75\text{ Å}$
	3.35	h_0	s (sh)	π -Stacking	$Z=2, N=1$
	21.75	001	vs (sh)	21.77	$T=140\text{ °C}$
	10.9	002	w (sh)	10.9	LamCol
	4.5	h_h	vs (br)	Alkyl chains	$d=21.77\text{ Å}$
	3.5	h_0	vs (sh)	π -Stacking	$A=87.3\text{ Å}^2$

^a d_{exp} and d_{theo} are the experimentally measured and theoretical diffraction spacings. The distances are given in Å.

^b $[hkl]$ is the indexation of the reflections, and h_0, h_{h1}, h_{h2} and h_h are the various short-range periodicities determined by XRD corresponding to the stacking distance (h_0), the liquid-like or quasi-liquid-like order of the molten chains (h_{h1}, h_{h2} and h_h), respectively.

^c Intensity of the reflections: vs: very strong, s: strong, m: medium, w: weak; br and sh stand for broad and sharp reflections, respectively.

^d d_{theo} , the lattice parameters a and b or the periodicity d are deduced from the following mathematical expressions: for LamCol, $d = \sum d_{00l}/N_{00l}$ where N_{00l} is the number of 00l reflections and for LamCol_r, $1/d_{hk} = \sqrt{((a/h)^2 + (b/k)^2)}$.

^e S is the lattice area, $S=a \times b$, and S_{col} , the columnar cross-section, $S_{\text{col}}=a \times b/2$. V_{mol} is the molecular volume; h is the intracolumnar repeating distance, deduced directly from the measured molecular volume and the columnar cross-section according to $h=ZV_{\text{mol}}/S=Nv_{\text{mol}}/S_{\text{col}}$. (Z is the number of molecules per lattice, N : number of molecules per periodic stacks; here $Z=2, N=1, V_{\text{mol}}=1900\text{ Å}^3$); A is the molecular area, $A=V_{\text{mol}}/d$.

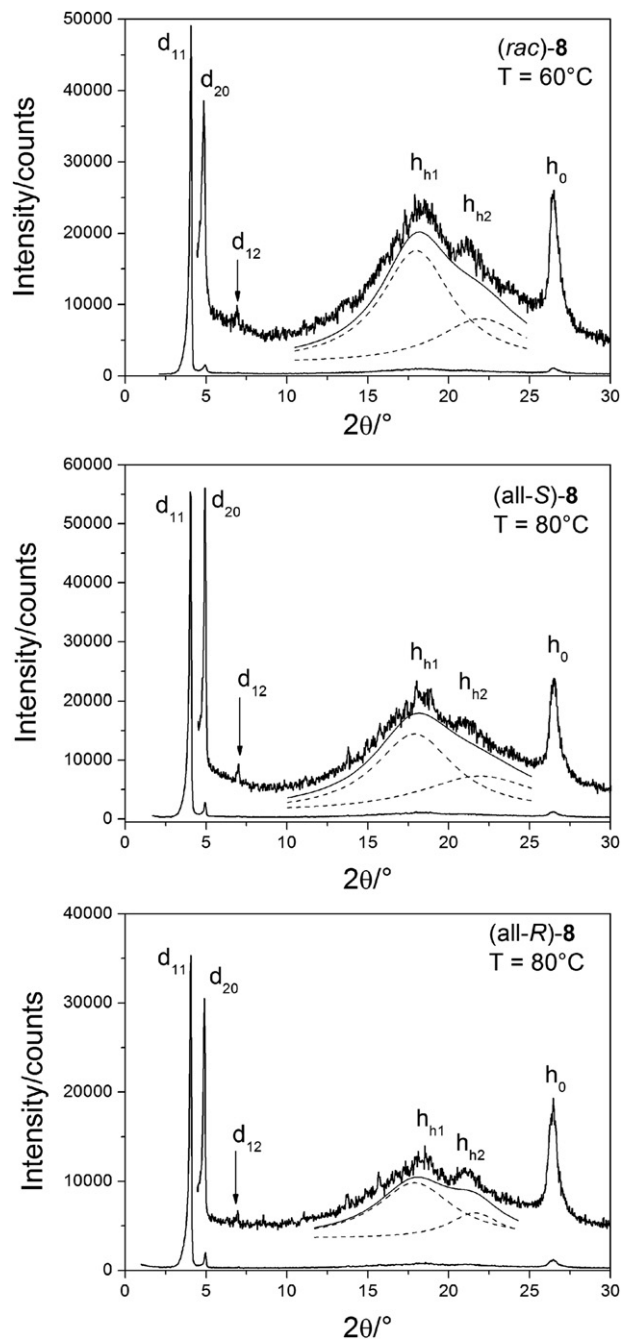


Fig. 5. Diffractograms of (*rac*)-**8** (top), (*all-R*)-**8** (middle), and (*all-S*)-**8** (bottom) of the low-temperature LamCol_r phase.

well-developed π -stacking of the mesogens into columns (correlation length from Scherrer formula: $\xi \sim 170\text{ Å}$, i.e., 50 stacked macrocycles). In the small-angle region, two first order reflections testify for a rectangular columnar ordering, and thanks to the presence of an additional higher-order reflection, the assignment of the three observed reflections to the (11), (20), and (12) reflections of the lattice is unambiguous. Within the two columns contained in the rectangular lattice, the macrocycles stack without significant out-of-plane tilting, as shown by the absence of significant difference between the molecular stacking distance, h_0 , and the intracolumnar periodicity, h , deduced from the estimated molecular volume (by assuming a density of 1.0 g cm^{-3}) and from the lattice area. The rectangular lattice is primitive, as shown by the (12), which excludes centered groups according the extinction rule

$h+k=2n+1$. The symmetry break between the columns can either result from a shift of the intercalated row from the lattice center or by a change of the columns themselves, presumably over alternating in-plane tilts. Depending upon the mechanism considered, three non-centered rectangular planar groups are theoretically compatible with the indexation of the observed reflections, namely $p2gg$, $p2mg$ and pg as displayed in Fig. 6.²⁰

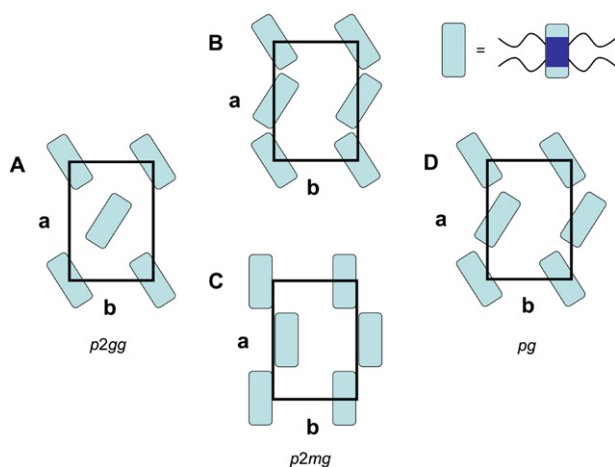


Fig. 6. Sketches representing the various non-centered, rectangular planar symmetries: A, $p2gg$; B and C: $p2mg$; D: pg (a and b are the lattice parameters, and the blue rectangle symbolizes the molecular cores, the chains being not represented for clarity).

The $p2gg$ lattice (Fig. 5) can be disregarded because of the high-intensity ratio between both the fundamental reflections (11) and (20) (Fig. 5). Indeed, this indicates that the electronic density contrast is strongly reduced along the a -vector lattice (low-intensity of the (20) reflection) and consequently that rows of columns stack in this direction with little or no intercalation of the low-electronic density aliphatic chains. This also implies that the tails are rejected between the rows, forming alternating strips of high- and low-electronic density. Thus, a lower packing symmetry ought to be considered. Considering first the $p2mg$ lattice (Fig. 6), two models are theoretically conceivable. For the first one, the columns are piled in a strict fashion along the a -vector with an alternation of the in-plane tilt, generating strips of chevron along the b -vector lattice. For the rectangular lattice, resulting from the undulations of the strips, one would expect a higher intensity contrast along the b -vector, and therefore high-intensity ($0l$) reflections. Although, the fact that the (12) higher-order reflection is the only one detected strongly suggests that the maximum electronic density contrast lies close, but is tilted from the b -lattice vector. This is however realized in the case of the other $p2mg$ model, whose glide plane occurs from a lateral shift between neighboring columns, consistent with the X-ray patterns. From a simple molecular point of view, this model does not appear satisfying, as interactions between vicinal columns stacked along the a -direction are not favored because of the lateral shift. On the contrary, the combination of lateral shifts and alternate tilts is consistent with the X-ray and molecular views, since interactions between the tips of the columns are restored. This leads to further symmetry breaking, and to the columns distribution according a pg lattice (Fig. 6).

It should be mentioned that long-time patterns recorded in both phases revealed additional very weak reflections corresponding to twice the first order periodicities (Fig. S3, Supplementary data). Stricto sensu, the real size of the lattices should then be a multiple of the lattices described above, but since these additional signals arise from minute deviations in the respective location/orientation between second neighboring columns, it is nevertheless more

convenient to use the small lattice periodicities for the description of the supramolecular organization.

On further heating, the three compounds also cross a transition to the same high-temperature mesophase with similar lattice parameters (Table 1, Fig. 7). In this phase, the persistence of the intense reflection attributed to the π -stacking of the macrocycles ($h_0 \sim 3.5$ Å; $\xi \sim 90$ Å, i.e., 25 mesogens) demonstrates the persistence of the columns. However the registry of the columns vanishes and the small-angle region just contains reflections occurring from the lamellar piling, i.e., a first order reflection with a periodicity close to the one of the (11) reflection in the former mesophase and the first harmonics. The structure of the mesophase is therefore similar to lamello-columnar organizations shown by smectic materials,^{6f,21}

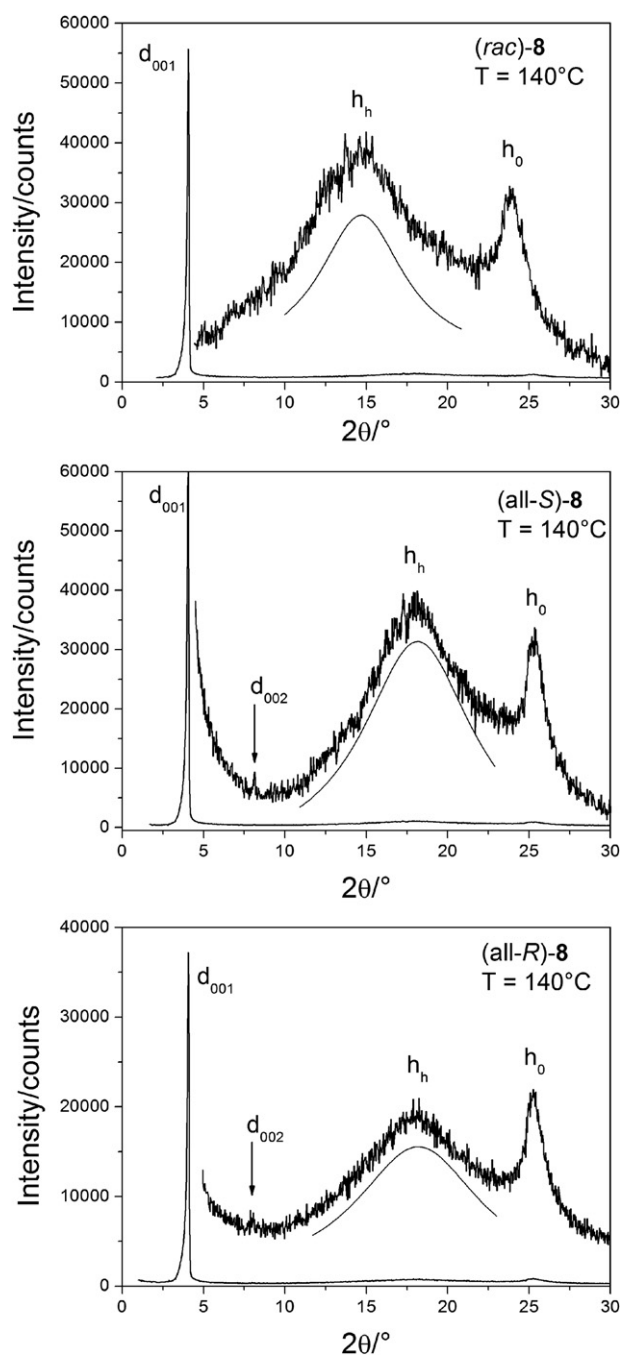


Fig. 7. Diffraction patterns of *rac*-**8** (top), (*all-R*)-**8** (middle), and (*all-S*)-**8** (bottom) of the high-temperature LamCol phase.

consisting in sublayers of stacked mesogens alternating with aliphatic sublayers. Since the orientation of these mesogens stacks varies beyond correlation distances, this mesophase appears uniaxial, as evidenced by polarizing microscopy. With the assumption of an untilted stacking within the columns, the average inter-columnar distance in the sublayers is estimated to $V/d/h_0 \sim 25 \text{ \AA}$, which is close to the distance between columns in the $\{11\}$ plane ($\sim 23 \text{ \AA}$) and that along the b -lattice vector (27 \AA), distances prefiguring the layers in the low-temperature mesophase. Another difference between both mesophases concerns the π -stacking distance, which changes from a value close to the minimum one in crystalline phases (3.3 \AA) to slightly larger values, which are typical for columnar phases of discotic macrocycles.²² As expected, this change toward more classical stacking distances is concomitant to a change toward more classical correlation lengths. Moreover, presumably because of the steric constraints connected to the unusual close packing of macrocycles in the low-temperature mesophase, the diffuse scattering of the molten aliphatic chains differs from the classical profile, consisting of a broad cusp-like band with a maximum at about 4.5 \AA (h_h). Thus, two maxima at about $4.1\text{--}4.2 \text{ \AA}$ (h_{h2}) and 4.8 \AA (h_{h1}) are observed instead, which should reveal a symmetry break in the average close packing of the proximal aliphatic segments. This would merit a nearer investigation, but the connection to the close packing of the macrocycle is certain, since the classical shape of the diffuse scattering is recovered in the high-temperature mesophase.

2.4. ECD and UV–vis spectroscopy

Chiroptical properties of chiral discotics (all-*S*)-**8** and (all-*R*)-**8** were investigated by electronic circular dichroism spectroscopy (ECD). The results obtained are collected in Fig. 8 together with UV–vis spectra of both solution and films prepared on quartz slides. The UV–vis spectrum of the thin film of **8** shows no significant differences in comparison with the solution spectrum. In general, absorption bands associated with the aromatic core occur in the same energy range, however, they are slightly broadened and red shifted in the case of the thin film (Fig. 8A, bottom).

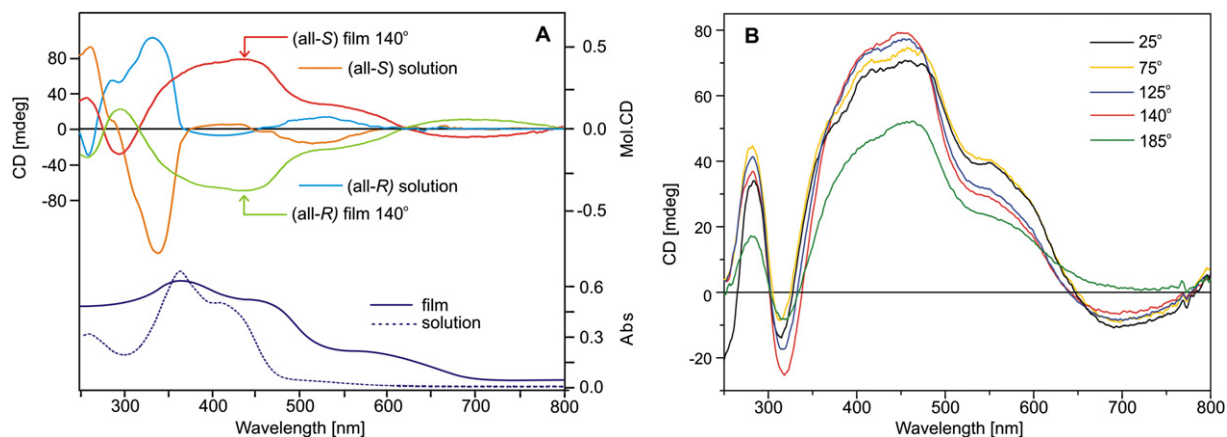


Fig. 8. (A) Comparison of ECD spectra of **8** in the LamCol mesophase and in dichloromethane solution (top) and UV–vis spectra of solution and thin film (bottom); (B) variable-temperature ECD spectra of (all-*S*)-**8** drop-casted films.

Much more fundamental differences are observed in the ECD spectra. As can be seen in Fig. 8A, the ECD spectrum recorded in dichloromethane indicates the presence of four relatively weak Cotton effects (CEs), located at around 540, 410, 340, and 260 nm, respectively. As expected, the effects are rather weak or even very weak because of the distance between the stereogenic centers placed in the flexible side-chains and dibenzotetraaza[14]-annulene core.

Analysis of the solution and thin film spectra of **8** show differences in their shape and magnitude. Apart from the appearance of an additional ECD band at 700 nm in (all-*R*)- and (all-*S*)-thin film spectra of **8**, the signs of remaining CEs present in both solution and thin film spectra are opposite with one exception, namely the band at 410 nm. Furthermore, compared with the spectra in solution the CEs of films of **8** are relatively strong, both at ambient and higher temperatures (Fig. 8B). The temperature-dependent data monitored as a dependence of ellipticity at 454 nm (in mdeg) on temperature indicated their good stability from ambient temperature up to $140 \text{ }^\circ\text{C}$. Further heating causes slow decomposition of the system, which is expressed by a reduced intensity of ECD bands at temperatures above $185 \text{ }^\circ\text{C}$ and by the disappearance of ECD band at 700 nm.

The above-mentioned behavior strongly suggests the creation of a chiral superstructure in which molecules are highly ordered enabling the occurrence of CEs. Moreover, the practically identical intensity of the ECD bands of the thin film at different temperatures suggest a similar type and degree of self-organization of individual chiral molecules. Since the ECD spectra of drop-casted thin films differ to a large extent from those obtained for the solutions, it seems reasonable to assume that chiroptical activity of the lamello-columnar mesophases results from a helical stacking of the molecules, induced and controlled by the chiral tails attached to the macrocyclic units.

2.5. Theoretical modeling

Additional support for such a conclusion may be obtained from the ECD spectra calculated at the B3LYP/3-21G for n -mers of (all-*S*)-**8** ($n=1, 2, 3$, and 4) with different twist angles (Fig. 9). Evolution of the spectrum with increasing n shows that for twisted oligomers ($\varphi=-30^\circ$ or 150°) negative CD band appears between 600 and 700 nm, in agreement with experimental CD spectrum of thin film. Conversely, for untwisted structures CD values at these wavelengths are positive. Thus, the CD spectra calculated for twisted structures reproduce the experimental data at long wavelengths and therefore exclude the untwisted molecular stacking.

Single-point energies calculated for dimers of (all-*S*)-**8** at the B97D/6-31+C** level for a molecular distance of 3.5 \AA and different twist angles show that the potential energy profile exhibits two minima: one for $\varphi=141^\circ$ and the other, with energy only 3 kcal/mol higher, at $\varphi=-11^\circ$ (Fig. 10). The energy of the untwisted dimer ($\varphi=0^\circ$) is remarkably higher, by about 800 kcal/mol. Such behavior results from steric repulsion between the aliphatic chains and/or benzoyl groups, which is minimized for twist angles close to -10°

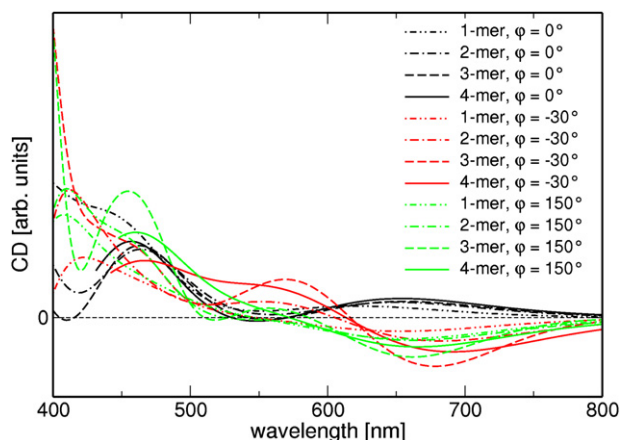


Fig. 9. Electronic CD spectra calculated at B3LYP/3-21G level for (all-*S*)-**8** dimers, trimers, and tetramers with different twist angles. CD values for *n*-mer were scaled by factor $1/n$.

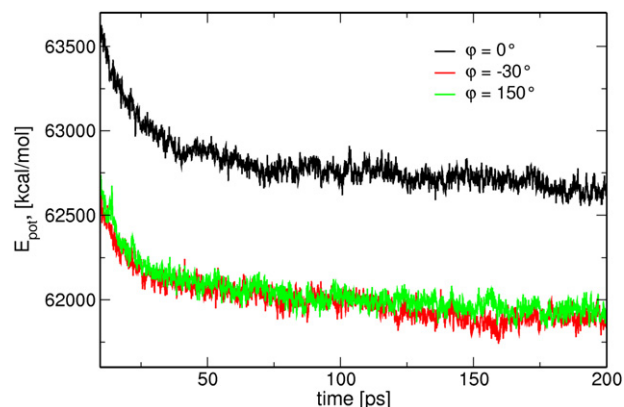


Fig. 11. Typical plot of potential energy changes in MD simulation for systems of 12 columns \times 12 (all-*S*)-**8** molecules with different values of initial column twist.

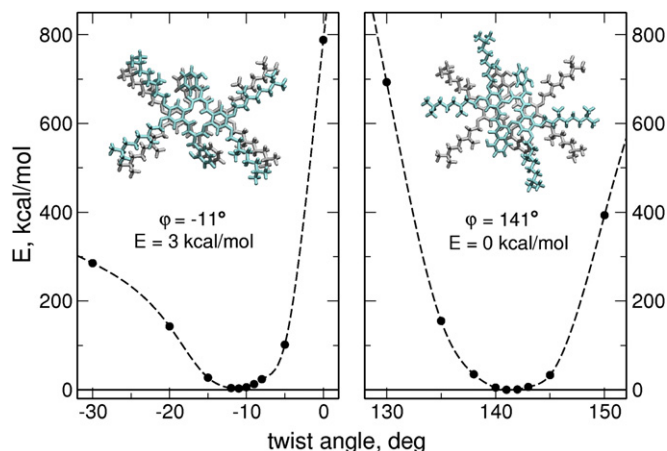


Fig. 10. Dependence of the potential energy calculated at the B97D/6-31+G** level on the twist angle ϕ for (all-*S*)-**8** dimer with 3.5 Å distance between molecular planes. Energy values are given relative to the lowest minimum.

and 140°. Although this suggests that the helical twist of the column of molecules is preferred, one should note that this result was obtained for frozen molecular geometry, optimized in B3LYP/6-31G** calculations. In real structures molecules will adapt their geometry to minimize the energy of the system.

To test the twisting in more realistic systems, we performed MD simulations for structures with columns of (all-*S*)-**8** twisted by 0°, -30° or 150° . Such twist angle values were chosen because for 12 molecules in column they commensurate with periodic boundary conditions of the simulation box. Spacing between molecules was 3.5 Å in all structures. In the course of simulations untwisted structures were unstable—we observed shifts and twists of the molecules leading to disorder in the column. Moreover, potential energy of the initially untwisted structures was higher than for twisted columns; in the latter case there was no significant difference between the two twist angles. A typical plot of potential energy is shown in Fig. 11. Snapshots from the MD trajectories for LamCol_r and LamCol structures are displayed in Figs. 12 and 13, respectively. Therefore, both quantum-chemical energy calculations and Molecular Dynamics simulations lead to the conclusion that twisted columns are favored.

At this point, it is interesting to compare data obtained from all these experiments. The twisted association between neighboring

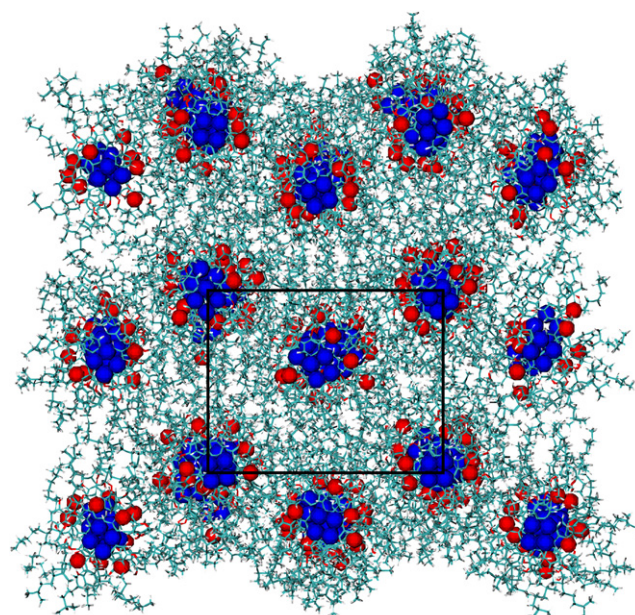


Fig. 12. Snapshot of the LamCol_r phase of (all-*S*)-**8** after about 0.1 ns of MD simulation. View of the local arrangement of the columns in the *pg* lattice.

molecules calculated by conformational geometry optimization, and confirmed by ECD measurements, leads to their helicoidal stacking into columns with a shift along the columnar axis as evidenced by MD calculations (Fig. 12). This helicoidal wrapping around the columnar axis produces in the lattice cross-plane *a* offset from the lattice center and the change of the molecular orientation, in consistency with the columnar *pg* lattice deduced by the XRD measurements. The particular molecular structure of the mesogens, i.e., a chain deficit with respect to a classical discotic molecule and the presence of two H-bonding sites at both extremities, leads to the anisotropic arrangement of columns. In the low-temperature phase, the rows of columns are almost continuous in one direction (*a*-lattice vector), as evidenced by both XRD and MD. In the high-temperature phase, the aliphatic chains are completely expelled from the rows, forming lamellae of columns alternating with layers of chains (Fig. 13). Finally, the effect of the chirality is restricted to mixing effect, i.e., the decrease of the melting and of the LamCol_r-to-LamCol transition temperatures in the racemic mixture with respect to the enantiomers, but has no significant impact on the supramolecular organization.

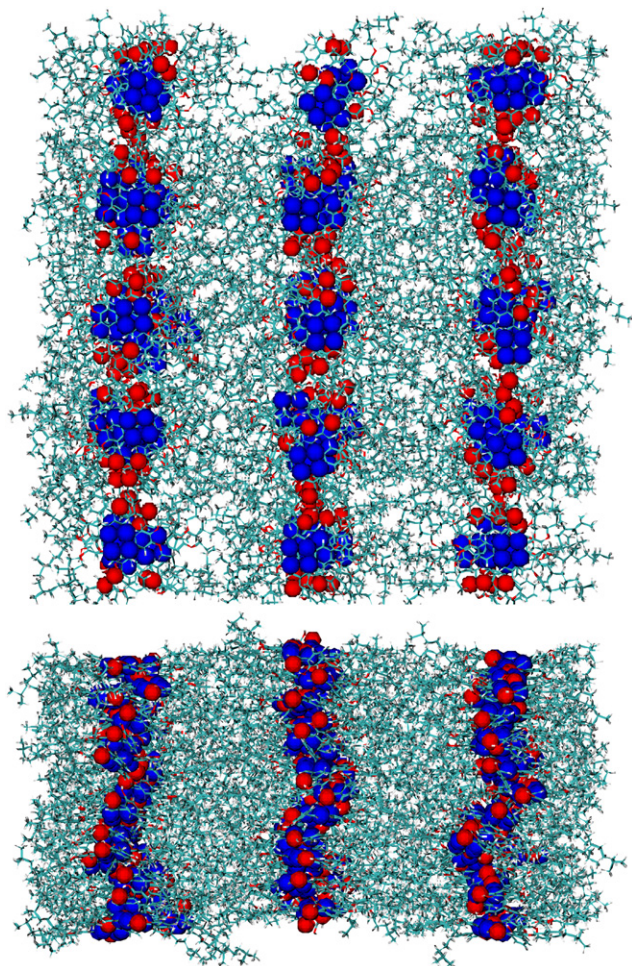


Fig. 13. Top and side views of the LamCol phase of (all-*S*)-**8** after about 0.1 ns of MD simulation.

3. Conclusions

New chiral mesogens were prepared, based on a DBTAA macrocyclic core, substituted at the periphery by four chiral (*R*)- and (*S*)-3,7-dimethyloctoxy groups and two 2-hydroxybenzoyl *meso* substituents. A lamello-columnar mesomorphism of sanidic-type has been assigned to the new materials on the basis of SA-XRD and DSC measurements, as well as of POM observations. Chiroptical properties of the drop-casted thin film were examined with use of temperature-variable ECD spectroscopy and compared with those of the solution. The results were interpreted in terms of a helical organization of the molecules in the mesophases, induced and controlled by the chiral and bulky substituents attached to the macrocyclic units. Experimental results have been supported by theoretical modeling using quantum-chemical calculations and MD simulations.

4. Experimental

4.1. General

Elemental analyses were performed on a CHNS Vario MICRO Cube microanalyzer. ^1H and ^{13}C NMR were run on a Bruker AMX (500 MHz) spectrometer. Chemical shifts (δ) are expressed in parts per million and *J* values in hertz. Signal multiplicities are denoted as s (singlet), d (doublet), t (triplet), q (quartet), and m (multiplet). ESI and MALDI-TOF mass spectra were taken on Esquire 3000 and

Bruker Reflex IV spectrometers, respectively. The IR spectra were recorded in KBr with a Bruker IFS 48 spectrophotometer. Melting points were measured using a Boethius apparatus and were uncorrected.

The transition temperatures and enthalpies were measured by differential scanning calorimetry with a TA Instruments DSC-Q1000 instrument operated at a scanning rates of 1–5 °C min⁻¹ on heating and on cooling.

The TGA measurements were carried out on a SDTQ 600 apparatus at scanning rate of 10 °C min⁻¹.

The XRD patterns were obtained with two different experimental set-ups (I, II). In all cases, a linear monochromatic Cu K α 1 beam ($\lambda=1.5405$ Å) was obtained using a sealed-tube generator (900 W) equipped with a bent quartz monochromator. In all cases, the crude powder was filled in Lindemann capillaries of 1 mm diameter and 10 μm wall-22 thickness. The initial set of diffraction patterns (I) was recorded with a curved Inel CPS 120 counter gas-filled detector linked to a data acquisition computer; periodicities up to 70 Å can be measured, and the sample temperature controlled to within ± 0.01 °C from 20 to 200 °C. Alternatively, patterns were also recorded on an image plate; periodicities up to 120 Å can be measured (scanned by STORM 820 from Molecular Dynamics with 50 μm resolution). The second set of diffraction patterns (II) was recorded on an image plate, where periodicities from 25 up to 350 Å can be measured, and the sample temperature controlled to within ± 0.1 °C from 20 to 200 °C. In each case exposure times were varied from 1 to 24 h.

A Zeiss Axio Scope A1 polarizing microscope combined with Linkam LTSE 420 hot stage, LNP95 cooling system, Linkam T 95 central processor, and Canon EOS 7D camera were used to characterize optical textures.

UV–vis absorption spectra were recorded with a Cary 100 UV–vis spectrometer and electronic circular dichroism spectra with a JASCO J-815 spectrophotometer. For solution measurements, dichloromethane for spectroscopy UVsol(TM) from MERCK was used as a solvent. Dichloromethane solutions with concentrations of 2.3×10^{-4} mol dm⁻³ or 2.5×10^{-4} mol dm⁻³ were examined in quartz cells with a path length of 0.1 or 2 cm with a band width of 2.0 nm, response 1 s, scanning speed 50 nm/s and five accumulations per spectrum. For thin film (solid state) measurements the neat samples were prepared by drop-casting from dichloromethane solution onto quartz plates. To avoid artifacts due to linear dichroism or/and linear birefringence, the quartz plates were rotated in a plane perpendicular to the light beam and the final ECD spectrum was the average of six spectra rotated through successive 60°, as proposed by Kuball et al.²³

Temperature ECD spectra were recorded on thin film deposited on a quartz plate with a JASCO J-715 spectrophotometer equipped with a Specac Variable Temperature Cell Holder.

4.2. Computational methods

Molecular modeling has been performed for the all-*S* enantiomer of compound **8**. Gaussian 09 rev. A.02²⁴ was used in quantum-chemical calculations reported in this work. Geometry of single (all-*S*)-**8** molecule was optimized in the density functional theory calculations with B3LYP functional and 6-31G** basis set. To find the preferred values of the twist angle in columns of **8**, single-point energies were computed for dimers of (all-*S*)-**8** with the 3.5 Å distance between molecular planes and varying twist angle ϕ . For better reproduction of interaction energies these calculations employed the 6-31+G** basis set and the B97D functional including semiempirical dispersion correction.²⁵ Electronic circular dichroism spectra of single molecules, dimers, trimers, and tetramers were calculated within the TDDFT methodology at the B3LYP/3-21G level; the size of the basis set was decreased to reduce the

computational cost. Structures of *n*-mers were obtained after applying a short energy minimization procedure in MM3 force field (see below) to the column of (all-*S*)-**8** molecules. Tinker v 4.2 modeling package²⁶ and all-atom MM3 force field was used in Molecular Dynamics. Simulations were performed for 4 or 12 stacks of 12 (all-*S*)-**8** molecules with periodic boundary conditions in all directions. Positions of the columns in the initial structures were chosen consistently with crystallographic data for LamCol_r or LamCol phase. The NVT ensemble with Berendsen thermostat was used, the temperature was set to 350 or 410 K for rectangular and lamcol structures, respectively. Timestep in simulations was 1 fs, length of MD runs was at least 0.1 ns.

4.3. Syntheses

(*S*)-(–)-β-Citronellol (*S*)-**2**, *R*-(+)-Pulegone, and other chemicals (Pd/C, NaBH₄, catechol, 3-formylchromone) were purchased from commercial sources and were used as received. (*R*)-(+)-β-Citronellol, (*R*)-**2**, and bromide **4** were synthesized as described in the literature.¹⁸ Compounds **3**, **5**, and **6** were prepared according to reported procedures.^{15,16,19} The solvents were dried using standard methods and were freshly distilled before use.

4.3.1. (*S,S*)-1,2-Dinitro-4,5-bis(3,7-dimethyloctoxy)benzene (*S,S*)-6**.** A solution of (*S*)-**5** (2.0 g, 5.1 mmol) in dichloromethane (30 mL) was added, dropwise, to vigorously stirred, concentrated nitric acid (10 mL) over a period of 30 min. Concentrated sulfuric acid (5 mL) was then added in stages and the stirring of the reaction mixture was continued for 1.5 h at room temperature. The reaction mixture was next poured onto crushed ice and the resultant suspension was extracted with dichloromethane (2 × 30 mL). The combined extracts were washed thoroughly, first with saturated aqueous sodium carbonate, then with water, twice, and were next dried over anhydrous MgSO₄. The solvent was removed under reduced pressure to leave a yellow solid, which was recrystallized from ethanol to give pale-yellow crystals of (*S,S*)-**6** (1.9 g, 76%), mp 81–82 °C, [α]_D²⁰ –3.91 (c 2.00, CH₂Cl₂). ¹H NMR (300 MHz, CDCl₃, δ ppm): 0.87 (d, *J*=6.6 Hz, 12H, H^{h,i}), 0.96 (d, *J*=6.4 Hz, 6H, H^j), 1.1–2.0 (m, 18H, H^{b,c,d,e,f}), 4.13 (m, 2H, H^g), 4.13 (t, *J*=6.5 Hz, 4H, H^a), 7.30 (s, 2H, H^{2,5}); ¹³C NMR (75 MHz, CDCl₃, δ ppm): 19.6 (C^j), 22.6, 22.7 (C^{h,i}), 24.7, 28.0, 29.9, 35.6, 37.2, 39.2 (C^{b,c,d,e,f,g}), 68.7 (C^a), 107.8 (C^{2,5}), 136.5 (C^{1,6}), 151.8 (C^{3,4}); ESI-MS *m/z* 481.3 (M+1)⁺; IR (KBr) ν_{\max} (cm⁻¹): 3072, 2957, 2925, 2869, 2844, 1538, 1221, 1046, 874. Anal. Calcd for C₂₆H₄₄N₂O₆: C, 65.0; H, 9.2; N, 5.8. Found: C, 65.0; H, 9.0; N, 5.8%.

4.3.2. (*R,R*)-1,2-Dinitro-4,5-bis(3,7-dimethyloctoxy)benzene (*R,R*)-6**.** (*R,R*)-**6** was synthesized analogously to the procedure described above, starting from (*R,R*)-**5**.

Yield 1.6 g, 65%, mp 81–82 °C, [α]_D²⁰ +4.39 (c 2.00, CH₂Cl₂). ¹H NMR (300 MHz, CDCl₃, δ ppm): 0.80 (d, *J*=6.6 Hz, 12H, H^{h,i}), 0.89 (d, *J*=6.4 Hz, 6H, H^j), 1.1–1.7 (m, 18H, H^{b,c,d,e,f}), 1.82 (m, 2H, H^g), 4.06 (t, *J*=6 Hz, 4H, H³), 7.23 (s, 2H, H^{2,5}); ¹³C NMR (75 MHz, CDCl₃, δ ppm): 20.2 (Cⁱ), 23.2, 23.3 (C^{h,i}), 25.3, 28.6, 30.5, 36.2, 37.8, 39.7 (C^{b,c,d,e,f,g}), 69.3 (C^a), 108.4 (C^{2,5}), 137.1 (C^{1,6}), 152.4 (C^{3,4}); ESI-MS: *m/z* 481.3 (M+1)⁺; IR (KBr) ν_{\max} (cm⁻¹): 3073, 2957, 2927, 2871, 2845, 1528, 1223, 1048, 875. Anal. Calcd for C₂₆H₄₄N₂O₆: C, 65.0; H, 9.2; N, 5.8. Found: C, 65.1; H, 9.5; N, 5.8%.

4.3.3. 2,3,11,12-Tetrakis((*S*)-3,7-dimethyloctoxy)-7,16-bis(2-hydroxybenzoyl)-5,14-dihydrodibenzo[b,i][1,4,8,11]-tetraazacyclotetradecine (all-*S*)-8**.** Powdered NaBH₄ (1.59 g, 42 mmol) was added to a reaction mixture containing **6** (1 g, 2.1 mmol) and 10% Pd/C (0.2 g) in methanol (75 mL), slowly and in small amounts, so as to maintain the gentle boiling of the mixture until the supernatant solution became colorless (about 30 min). The catalyst, solid by-products, and excess undissolved NaBH₄ were removed by means

of filtration through a pad of Celite under argon. 3-Formylchromone (0.36 g, 2.1 mmol) was immediately added to the filtrate and the mixture was allowed to reflux under argon for 2 h. The crude product, which precipitated after cooling was filtered off and recrystallized from acetone/methanol (4:1) to give brown crystals of (all-*S*)-**8** (0.49 g, 40.8%), mp 192 °C. ¹H NMR (300 MHz, CDCl₃, δ ppm): 0.87 (d, *J*=6.6 Hz, 24H, H^{h,i}), 0.94 (d, *J*=6.3 Hz, 12H, H^j), 1.1–1.4 (m, 24H, H^{d,e,f}), 1.5–1.7 (m, 12H, H^{b,c,g}), 1.84 (m, 4H, H^b), 3.96 (m, *J*=6.7 Hz, 8H, H^a), 6.64 (s, 4H, H^{1,4,10,13}), 6.88 (dd, *J*=7.5, 7.5 Hz, 2H, H^{2,4}), 7.06 (d, *J*=7.8 Hz, 2H, H^{2,2}), 7.44 (dd, *J*=7.8, 7.8 Hz, 2H, H^{2,3}), 7.54 (d, *J*=7.8 Hz, 2H, H^{2,5}), 8.34 (d, *J*=6 Hz, 4H, H^{6,8,15,17}), 11.36 (s, 2H, OH²¹), 14.95 (t, *J*=6.6 Hz, 2H, H^{N5,N14}); ¹³C NMR (75 MHz, CDCl₃, δ ppm): 19.7 (C^j), 22.7, 22.8 (C^{h,i}), 24.8 (C^e), 28 (C^g), 30.0 (C^c), 36.3 (C^b), 37.5 (C^d), 39.4 (C^f), 68.1 (C^a), 100.7 (C^{1,4,10,13}), 109.0 (C²⁰), 118.2 (C^{2,4}), 118.5 (C^{2,2}), 120.3 (C^{7,16}), 130.2 (C^{5a,9a,14a,18a}), 131.2 (C^{2,5}), 134.7 (C^{2,3}), 148.7 (C^{2,3,11,12}), 150.8 (C^{6,8,15,17}), 161.6 (C²¹), 196.0 (C¹⁹); IR (KBr) ν_{\max} (cm⁻¹): 2955, 2927, 2869, 1639, 1522, 1258, 1011, 816; MALDI-MS: *m/z* 1152.5 M⁺. Anal. Calcd for C₇₂H₁₀₄N₄O₈: C, 74.96; H, 9.1; N, 4.86. Found: C, 74.9; H, 9.0; N, 4.8%.

4.3.4. 2,3,11,12-Tetrakis((*R*)-3,7-dimethyloctoxy)-7,16-bis(2-hydroxybenzoyl)-5,14-dihydrodibenzo[b,i][1,4,8,11]-tetraazacyclotetradecine (all-*R*)-8**.** The procedure was analogous to that described above. The product was recrystallized from acetone/methanol (4:1) to give brown crystals of (all-*R*)-**8** (0.44 g, 36.4%), mp 192 °C. ¹H NMR (300 MHz, CDCl₃, δ ppm): 0.87 (d, *J*=6.6 Hz, 24H, H^{h,i}), 0.94 (d, *J*=6.4 Hz, 12H, H^j), 1.1–1.4 (m, 24H, H^{d,e,f}), 1.5–1.7 (m, 12H, H^{b,c,g}), 1.83 (m, 4H, H^b), 3.93 (m, 8H, H^a), 6.58 (s, 4H, H^{1,4,10,13}), 6.86 (dd, *J*=7.5, 7.5 Hz, 2H, H^{2,4}), 7.05 (d, *J*=7.8 Hz, 2H, H^{2,2}), 7.43 (dd, *J*=7.8, 7.8 Hz, 2H, H^{2,3}), 7.51 (d, *J*=7.8 Hz, 2H, H^{2,5}), 8.28 (d, *J*=6 Hz, 4H, H^{6,8,15,17}), 11.33 (s, 2H, OH²¹), 14.95 (t, *J*=6.6 Hz, 2H, H^{N5,N14}); ¹³C NMR (75 MHz, CDCl₃, δ ppm): 19.7 (C^j), 22.6, 22.7 (C^{h,i}), 24.7 (C^e), 28.0 (C^g), 29.9 (C^c), 36.2 (C^b), 37.4 (C^d), 39.3 (C^f), 67.9 (C^a), 100.4 (C^{1,4,10,13}), 108.9 (C²⁰), 118.1 (C^{2,4}), 118.4 (C^{2,2}), 120.3 (C^{7,16}), 130.0 (C^{5a,9a,14a,18a}), 131.0 (C^{2,5}), 134.5 (C^{2,3}), 148.5 (C^{2,3,11,12}), 150.6 (C^{6,8,15,17}), 161.5 (C²¹), 195.8 (C¹⁹); MS (ESI) *m/z* 1153.5 (M+1)⁺; IR (KBr) ν_{\max} (cm⁻¹): 2955, 2927, 2869, 1639, 1522, 1258, 1011, 816. Anal. Calcd for C₇₂H₁₀₄N₄O₈: C, 74.96; H, 9.1; N, 4.86. Found: 75.05; H, 9.3; N, 4.95%.

Acknowledgements

Financial Support from the Polish Ministry of Science and Higher Education (Project NN204 333437) is gratefully acknowledged. The research was carried out with the equipment purchased thanks to the financial support of the European Regional Development Fund in the framework of the Polish Innovation Economy Operational Program (contract no. POIG.02.01.00-12-023/08). B.H. and B.D. thank the CNRS for support.

Supplementary data

TGA and DSC results, SA-XRD pattern of the two phases of (all-*S*)-**8**, schematic representation of the structures of the mesophases. Supplementary data associated with this article can be found in the online version, at doi:10.1016/j.tet.2012.03.037.

References and notes

- (a) Sergeev, S.; Pisula, W.; Geerts, Y. H. *Chem. Soc. Rev.* **2007**, *36*, 1902; (b) Christ, T.; Glösen, B.; Greiner, A. J.; Kettner, A.; Sander, R.; Stümpflen, V.; Tsukruk, V.; Wendorff, J. H. *Adv. Mater.* **1997**, *9*, 48; (c) Bisoyi, H. K.; Kumar, S. *Chem. Soc. Rev.* **2010**, *39*, 264; (d) van de Witte, P.; Brehmer, M.; Lub, J. J. *Mater. Chem.* **1999**, *9*, 2087; (e) Boden, N.; Bushby, R. J.; Clements, J.; Movaghar, B. J. *Mater. Chem.* **1999**, *9*, 2081; (f) Hassheider, T.; Benning, S. A.; Kitzzerow, H.-S.; Achard, M.-F.; Bock, H. *Angew. Chem., Int. Ed.* **2001**, *40*, 2060; (g) Hassheider, T.;

- Benning, S. A.; Lauhof, M. W.; Kitzerow, H. S.; Bock, H.; Watson, M. D.; Müllen, K. *Mol. Cryst. Liq. Cryst.* **2004**, *413*, 2597; (h) O'Neill, M.; Kelly, S. M. *Adv. Mater.* **2003**, *15*, 1135; (i) Kato, T.; Yasuda, T.; Kamikawa, Y.; Yoshio, M. *Chem. Commun.* **2009**, 729; (j) Kumar, S. *Chem. Soc. Rev.* **2006**, *35*, 83; (k) Pisula, W.; Zorn, M.; Young, J. C.; Müllen, K.; Zentel, R. *Macromol. Rapid Commun.* **2009**, *30*, 1179; (l) Kaafarani, B. R. *Chem. Mater.* **2011**, *23*, 378.
- (a) Adam, U. *Prog. Polym. Sci.* **2003**, *28*, 1049; (b) Takezoe, H.; Kishikawa, K.; Gorecka, E. *J. Mater. Chem.* **2006**, *16*, 2412; (c) Vera, F.; Serrano, J. L.; Sierra, T. *Chem. Soc. Rev.* **2009**, *38*, 781; (d) Keizer, H. M.; Sijbesma, R. P. *Chem. Soc. Rev.* **2005**, *34*, 226.
 - (a) Bock, H.; Helfrich, W. *Liq. Cryst.* **1992**, *12*, 697; (b) Bock, H.; Helfrich, W. *Liq. Cryst.* **1995**, *18*, 387; (c) Bock, H.; Helfrich, W. *Liq. Cryst.* **1995**, *18*, 707; (d) Barbera, J.; Iglesias, R.; Serrano, J. L.; Sierra, T.; de la Fuente, M. R.; Palachios, B.; Perez-Jubindo, M. A.; Vazquez, J. T. *J. Am. Chem. Soc.* **1998**, *120*, 2908; (e) Scherowsky, G.; Chen, X. H. *J. Mater. Chem.* **1995**, *5*, 417.
 - (a) Adam, D.; Schuhmacher, P.; Simmerer, J.; Häußling, L.; Siemensmeyer, K.; Etbach, K. H.; Ringsdorf, H.; Haarer, D. *Nature* **1994**, *371*, 141; (b) van de Craats, A. M.; Warman, J. M.; Fechtenkötter, A.; Brand, J. D.; Harbison, M. A.; Müllen, K. *Adv. Mater.* **1999**, *11*, 1469; (c) Fechtenkötter, A.; Saalwächter, K.; Harbison, M. A.; Müllen, K.; Spiess, H. W. *Angew. Chem., Int. Ed.* **1999**, *38*, 3039; (d) Warman, J. M.; de Haas, M. P.; Dicker, G.; Grozema, F. C.; Pirus, J.; Debije, M. G. *Chem. Mater.* **2004**, *16*, 4600; (e) Iino, H.; Takayashiki, Y.; Hanna, J.; Bushby, R. J.; Haarer, D. *Appl. Phys. Lett.* **2005**, *87*, 192105; (f) Rohr, U.; Kohl, C.; Müllen, K.; van de Craats, A.; Warman, J. *J. Mater. Chem.* **2001**, *11*, 1789; (g) Isoda, K.; Yasuda, T.; Kato, T. *Chem. Asian J.* **2009**, *4*, 1619.
 - (a) Kauranen, M.; Verbiest, T.; Boutton, C.; Teerenstra, M. N.; Clays, K.; Schouten, A. J.; Nolte, R. J. M.; Persoons, A. *Science* **1995**, *270*, 966; (b) Verbiest, T.; van Elshocht, S.; Kauranen, M.; Hellemans, L.; Snauwaert, J.; Nuckolls, C.; Katz, T. J.; Persoons, A. *Science* **1998**, *281*, 913; (c) Fox, J. M.; Katz, T. J.; van Elshocht, S.; Verbiest, T.; Kauranen, M.; Persoons, A.; Thongpanchang, T.; Krauss, T.; Brus, L. *J. Am. Chem. Soc.* **1999**, *121*, 3453; (d) Lee, H.; Kim, D.; Lee, H.-K.; Qiu, W.; Oh, N.-K.; Zin, W.-C.; Kim, K. *Tetrahedron Lett.* **2004**, *45*, 1019.
 - (a) Gregg, B. A.; Fox, M. A.; Bard, A. J. *J. Am. Chem. Soc.* **1989**, *111*, 3024; (b) Kimura, M.; Saito, Y.; Ohta, K.; Hanabusa, K.; Shirai, H.; Kobayashi, N. *J. Am. Chem. Soc.* **2002**, *124*, 5274; (c) Liu, C.; Bard, A. J. *Acc. Chem. Res.* **1999**, *32*, 235; (d) Castella, M.; Lopez-Calahorra, F.; Velasco, D.; Finkelmann, H. *Chem. Commun.* **2002**, 2348; (e) Sessler, J. L.; Callaway, W.; Dudek, S. P.; Date, R. W.; Lynch, V. L.; Bruce, D. W. *Chem. Commun.* **2003**, 2422; (f) Stepien, M.; Donnio, B.; Sessler, J. L. *Chem.—Eur. J.* **2007**, *13*, 6853.
 - (a) Piechocki, C.; Simon, J.; Skoulios, A.; Guillon, D.; Weber, P. *J. Am. Chem. Soc.* **1982**, *104*, 5245; (b) Chandrasekhar, S. *Mol. Cryst. Liq. Cryst.* **1981**, *63*, 171; (c) Binnemans, K.; Sleven, J.; De Feyter, S.; De Schryver, F. C.; Donnio, B.; Guillon, D. *Chem. Mater.* **2003**, *15*, 3930.
 - (a) Herwig, P.; Kayser, C. W.; Müllen, K.; Spiess, H. W. *Adv. Mater.* **1996**, *8*, 510; (b) Simpson, C. D.; Wu, J. S.; Watson, M. D.; Müllen, K. *J. Mater. Chem.* **2004**, *14*, 494; (c) Pisula, W.; Kastler, M.; Wasserfallen, D.; Mondeshki, M.; Pirus, J.; Schnell, I.; Müllen, K. *Chem. Mater.* **2006**, *18*, 3634; (d) Alameddine, B.; Aebischer, O. F.; Amrein, W.; Donnio, B.; Deschenaux, R.; Guillon, D.; Savary, C.; Scanu, D.; Scheidegger, O.; Jenny, T. A. *Chem. Mater.* **2005**, *17*, 4798.
 - (a) Rego, J. A.; Kumar, S.; Ringsdorf, H. *Chem. Mater.* **1996**, *8*, 1402; (b) Terasawa, N.; Monobe, H.; Kiyohara, K.; Shimizu, Y. *Chem. Commun.* **2003**, 1678; (c) Gramsbergen, E. F.; Hoving, H. J.; de Jeu, W. H.; Praefcke, K.; Kohne, B. *Liq. Cryst.* **1986**, *1*, 397; (d) Cammidge, A. N.; Gopee, H. *J. Mater. Chem.* **2001**, *11*, 2773; (e) Zelcer, A.; Donnio, B.; Bourgogne, C.; Cukiernik, F. D.; Guillon, D. *Chem. Mater.* **2007**, *19*, 1992.
 - (a) van Nostrum, C. F.; Bosman, A. W.; Gelinck, G. H.; Picken, S. J.; Schouten, P. G.; Warman, J. M.; Schouten, A.-J.; Nolte, R. J. M. *J. Chem. Soc., Chem. Commun.* **1993**, 1120; (b) Malthête, J.; Jacques, J.; Nguyen, H.-T.; Destrade, C. *Nature* **1982**, *298*, 46; (c) Levelut, A. M.; Oswald, P.; Ghanem, A.; Malthête, J. *J. Phys.* **1984**, *45*, 745.
 - (a) Ryu, J.-H.; Tang, L.; Lee, E.; Kim, H.-J.; Lee, M. *Chem.—Eur. J.* **2008**, *14*, 871; (b) Verbiest, T.; Sionke, S.; Persoons, A.; Vylicky, L.; Katz, T. J. *Angew. Chem., Int. Ed.* **2002**, *41*, 3882; (c) Barbera, J.; Bardaj, M.; Jimenez, J.; Laguna, A.; Martinez, M. P.; Oriol, L.; Serrano, J. L.; Zaragoza, I. *J. Am. Chem. Soc.* **2005**, *127*, 8994; (d) Ziessel, R. *Coord. Chem. Rev.* **2001**, *216/217*, 195; (e) Fontes, E.; Heiney, P. A.; de Jeu, W. H. *Phys. Rev. Lett.* **1988**, *61*, 1202; (f) Wu, J. S.; Watson, M. D.; Zhang, L.; Wang, Z. H.; Müllen, K. *J. Am. Chem. Soc.* **2004**, *126*, 177; (g) Levelut, A. M. *J. Phys. Lett.* **1979**, *40*, 81; (h) Lesac, A.; Donnio, B.; Guillon, D. *Soft Matter* **2009**, *5*, 4231; (i) Yang, C.-W.; Hsia, T.-H.; Chen, C.-C.; Lai, C.-K.; Liu, R.-S. *Org. Lett.* **2008**, *10*, 4069; (j) Gorecka, E.; Pocięcha, D.; Mieczkowski, J.; Matraszek, J.; Guillon, D.; Donnio, B. *J. Am. Chem. Soc.* **2004**, *126*, 15946.
 - Grolik, J.; Sieroń, L.; Eilmes, J. *Tetrahedron Lett.* **2006**, *47*, 8209.
 - Grolik, J.; Dominiak, P. M.; Sieroń, L.; Woźniak, K.; Eilmes, J. *Tetrahedron* **2008**, *64*, 7796.
 - (a) van Nostrum, C. F.; Bosman, A. W.; Gelinck, G. H.; Schouten, P. G.; Warman, J. M.; Kentgens, A. P. M.; Devillers, M. A. C.; Meijerink, A.; Picken, S. J.; Sohling, U.; Schouten, A. J.; Nolte, R. J. M. *Chem.—Eur. J.* **1995**, *1*, 171; (b) Pisula, W.; Tomovic, Z.; Watson, M. D.; Müllen, K.; Kussmann, J.; Ochsenfeld, C.; Metzroth, T.; Gauss, J. *J. Phys. Chem. B* **2007**, *111*, 7481; (c) Malthête, J.; Levelut, A. M.; Liebert, L. *Adv. Mater.* **1992**, *4*, 37; (d) Bushey, M. L.; Nguyen, T.-Q.; Zhang, W.; Horoszewski, D.; Nuckolls, C. *Angew. Chem., Int. Ed.* **2004**, *43*, 5446; (e) Green, M. M.; Ringsdorf, H.; Wagner, J.; Wüstefeld, R. *Angew. Chem., Int. Ed. Engl.* **1990**, *29*, 1478; (f) Barbera, J.; Puig, L.; Romero, P.; Serrano, J. L.; Sierra, T. *J. Am. Chem. Soc.* **2005**, *127*, 458.
 - Mohr, B.; Enkelmann, V.; Wenger, G. *J. Org. Chem.* **1994**, *59*, 635.
 - Forget, S.; Veber, M.; Strzelecka, H. *Mol. Cryst. Liq. Cryst.* **1995**, *258*, 263.
 - Sigg, I.; Haas, G.; Winkler, T. *Helv. Chim. Acta* **1982**, *65*, 275.
 - Schouten, P. G.; van Der Pol, J. F.; Zwikker, J. W.; Drenth, W.; Picken, S. J. *Mol. Cryst. Liq. Cryst.* **1991**, *195*, 291.
 - Messmore, B. W.; Sukerkar, P. A.; Stupp, S. I. *J. Am. Chem. Soc.* **2005**, *127*, 7992.
 - International Tables for Crystallography*, 4th ed; Hahn, T., Ed.; The International Union of Crystallography, Kluwer Academic: Dordrecht, 1995; Vol. A.
 - (a) Haristoy, D.; Méry, S.; Heinrich, B.; Mager, L.; Nicoud, J.-F.; Guillon, D. *Liq. Cryst.* **2000**, *27*, 321; (b) Méry, S.; Haristoy, D.; Nicoud, J.-F.; Guillon, D.; Diele, S.; Monobe, H.; Shimizu, Y. *J. Mater. Chem.* **2002**, *12*, 37; (c) Mori, A.; Yokoo, M.; Hashimoto, M.; Ujiie, S.; Diele, S.; Baumeister, U.; Tschierske, C. *J. Am. Chem. Soc.* **2003**, *125*, 6620; (d) Pucci, D.; Barberio, G.; Crispini, A.; Francescangeli, O.; Ghedini, M.; La Deda, M. *Eur. J. Inorg. Chem.* **2003**, 3649; (e) Cardinaels, T.; Driesen, K.; Parac-Vogt, T. N.; Heinrich, B.; Bourgogne, C.; Guillon, D.; Donnio, B.; Binnemans, K. *Chem. Mater.* **2005**, *17*, 6589; (f) Cammerel, F.; Donnio, B.; Bourgogne, C.; Schmutz, M.; Guillon, D.; Davidson, P.; Ziessel, R. *Chem.—Eur. J.* **2006**, *12*, 4261; (g) Miao, J.; Zhu, L. *Chem. Mater.* **2010**, *22*, 197; (h) Wang, L.; Cho, H.; Lee, S.-H.; Lee, C.; Jeong, K.-U.; Lee, M.-H. *J. Mater. Chem.* **2011**, *21*, 60.
 - Levelut, A. M. *J. Chim. Phys.* **1983**, *80*, 149.
 - Kuball, H.-G.; Schoenhofer, A. In *Circular Dichroism: Principles and Applications*; Nakanishi, K.; Berova, N.; Woody, R., Eds.; VCH: New York, NY, 1994, Chapter 4.
 - Frisch, M. J.; Trucks, G. W.; Schlegel, H. B.; Scuseria, G. E.; Robb, M. A.; Cheeseman, J. R.; Scalmani, G.; Barone, V.; Mennucci, B.; Petersson, G. A.; Nakatsuji, H.; Caricato, M.; Li, X.; Hratchian, H. P.; Izmaylov, A. F.; Bloino, J.; Zheng, G.; Sonnenberg, J. L.; Hada, M.; Ehara, M.; Toyota, K.; Fukuda, R.; Hasegawa, J.; Ishida, M.; Nakajima, T.; Honda, Y.; Kitao, O.; Nakai, H.; Vreven, T.; Montgomery, J. A., Jr.; Peralta, J. E.; Ogliaro, F.; Bearpark, M.; Heyd, J. J.; Brothers, E.; Kudin, K. N.; Staroverov, V. N.; Kobayashi, R.; Normand, J.; Raghavachari, K.; Rendell, A.; Burant, J. C.; Iyengar, S. S.; Tomasi, J.; Cossi, M.; Rega, N.; Millam, J. M.; Klene, M.; Knox, J. E.; Cross, J. B.; Bakken, V.; Adamo, C.; Jaramillo, J.; Gomperts, R.; Stratmann, R. E.; Zazyev, O.; Austin, A. J.; Cammi, R.; Pomelli, C.; Ochterski, J. W.; Martin, R. L.; Morokuma, K.; Zakrzewski, V. G.; Voth, G. A.; Salvador, P.; Dannenberg, J. J.; Dapprich, S.; Daniels, A. D.; Farkas, Ö.; Foresman, J. B.; Ortiz, J. V.; Cioslowski, J.; Fox, D. J. *Gaussian 09, Revision A.02*; Gaussian: Wallingford CT, 2009.
 - Grimme, S. *J. Comput. Chem.* **2006**, *27*, 1787.
 - Tinker Molecular Modeling Package v. 4.2. <http://dasher.wustl.edu/tinker/>.